Dalton Transactions

ROYAL SOCIETY OF CHEMISTRY

PERSPECTIVE

Cite this: *Dalton Trans.*, 2020, **49**, 15548

Optimizing supramolecular interactions in metal–organic frameworks for C_2 separation

Gui-Fang Hua, Xiao-Jing Xie, Weigang Lu * and Dan Li *

C_2 separation is of great importance in the petrochemical industry. Traditionally, it is performed by distillation at cryogenic temperatures, which necessitates the consumption of a huge amount of energy to operate the refrigeration system in the production process. In this regard, it is imperative to seek alternative separation methods with high efficiency and low energy cost. Although of recent origin, metal–organic frameworks (MOFs) have already been extensively studied as advanced adsorbents in many applications, and significant progress has been made particularly in gas separation owing to their unprecedented porosity and tunable structures. In this review, we extrapolated three most frequently invoked design strategies for efficient C_2 separation hinged upon supramolecular interactions, including molecular sieving, gate opening, and surface engineering. Recent progress of MOF materials in C_2 separation was highlighted within each of these strategies, and their advantages and limitations are compared and discussed. Accordingly, we provide perspectives on current challenges and future emphases in designing MOF materials for hydrocarbon separation. With our continued efforts in this area, we expect that integrating supramolecular interactions in a single MOF system is a viable approach to achieve a balance between adsorption capacity and selectivity for different hydrocarbon separation scenarios.

Received 28th August 2020,
Accepted 1st October 2020

DOI: 10.1039/d0dt03013a

rsc.li/dalton

Introduction

Among C_2 hydrocarbons, ethylene (C_2H_4) is one of the most important industrial raw materials because of its use in the production of fundamental building blocks such as polyethylene, ethylene oxide, and ethylene chloride, *etc*. High-purity C_2H_4 is essential for the quality of these end-products. However, C_2H_4 is predominantly produced by steam cracking and the crude product usually contains impurities such as ethane (C_2H_6) and acetylene (C_2H_2). In particular, the presence of C_2H_2 will poison the catalysts, resulting in reduced quality of these C_2H_4 end-products. Therefore, further separation of C_2H_4 with high purity is critical for industrial production.

C_2 separation, as it turns out, is very difficult because of its similar physical and chemical properties.[1] Cryogenic distillation is predominantly used in industrial C_2H_4 purification and the technology is relatively mature. However, this process is

College of Chemistry and Materials Science, and Guangdong Provincial Key Laboratory of Functional Supramolecular Coordination Materials and Applications, Jinan University, Guangzhou 510632, P. R. China. E-mail: weiganglu@jnu.edu.cn, danli@jnu.edu.cn

Gui-Fang Hua

Gui-Fang Hua is pursuing her Master of Science degree in the College of Chemistry and Materials Science at Jinan University. Her research interests involve designing and synthesizing metal–organic frameworks and their applications in gas separation.

Xiao-Jing Xie

Xiao-Jing Xie received her M. Sc. degree in the College of Chemistry and Materials Science at Jinan University (2020). Her research focuses on the design and synthesis of metal–organic frameworks for gas separation.

extremely energy demanding due to the operation of the refrigeration system.[2] In contrast, adsorption-based separation by porous materials can be carried out at room temperatures with considerably reduced energy penalty; therefore, it may hold promise for replacing cryogenic distillation in hydrocarbon separation.[3] Conventional porous materials, such as zeolites and carbon-based materials, usually exhibit either poor adsorption selectivity or adsorption capacity for hydrocarbons, and not many of them have been demonstrated as promising in hydrocarbon separation.[4] Besides, the lack of flexibility in adjusting pore size/shape and surface functionalization limits their further improvement in separation performance.[5]

On the other hand, metal–organic frameworks (MOFs), also known as porous coordination polymers (PCPs), have recently emerged as coordination polymers assembled with metal ions/clusters and organic linkers.[6] By taking full advantage of reticular chemistry, MOFs have been demonstrating their unprecedented structural designability at the molecular level.[7–10] The geometry, size, and flexibility of the MOF frameworks can be adjusted by changing the identities of individual metal ions/clusters and organic linkers,[11–22] as evidenced by the fact that tens of thousands of different MOF structures have been reported in the last two decades.[23,24]

Currently, MOFs are gaining tremendous attention due to their superior performance in hydrocarbon separation. The potential of MOFs with custom-made pore geometry and surface functionalization for targeted gas separation in different scenarios has intrigued many researchers from both industry and academia. More than a few comprehensive reviews have recently been published on MOF-based adsorbents for hydrocarbon separation.[5,21,25–28] Herein, we focus on MOF materials in C_2 separation and highlight their recent progress from the perspectives of structural design. The three most frequently used design strategies have been extrapolated from recent literature according to their corresponding supramolecular interactions, including molecular sieving, gate opening, and surface engineering. Their advantages and limitations are compared and discussed (Fig. 1). With our continued efforts in this research field, we provide perspectives on current challenges and future emphases in the design of MOF materials for hydrocarbon separation. In particular, we expect that integrating supramolecular interactions is a viable approach to achieve a balance between adsorption capacity and selectivity for different hydrocarbon separation scenarios.

Molecular sieving

Molecular sieves are generally referred to as microporous materials with well-defined pore structures and can function as selective adsorbents for separating molecules of different sizes. Traditional molecular sieves, particularly zeolites, are well known in the adsorptive separation of small molecules, such as CO, CH_4, O_2, N_2, and H_2O, by excluding the ones with larger sizes. However, the lack of potential in adjusting pore size/shape and surface functionalization limits their applications in a broader range. Compared to traditional molecular sieves, MOF materials are far more superior in structural designability due to the numerous coordination configurations between metal clusters and organic linkers, which can be utilized to construct different pore sizes and geometric shapes to cater for different separation scenarios. Besides functioning as size-based molecular sieves, the potential of tuning the surface chemistry could render MOF materials in interaction-induced molecular sieves, preferentially adsorbing molecules exhibiting stronger host–guest interactions, not necessarily the small-sized ones.

Weigang Lu

Weigang Lu obtained his Ph.D. in Organic Chemistry (2002) and stayed as a lecturer at Sun Yat-Sen University (2002–2005). After a visiting scholar stint at the Hong Kong University of Science & Technology (2005–2008), he joined Texas A&M University as an assistant research scientist in Prof. Hong-Cai Zhou's group (2008–2015). He started independent research as a research specialist at Fayetteville State University (2016–2018) and now he is a professor of chemistry at Jinan University (2018–Present). His research interest focuses on the rational design and synthesis of porous materials for energy-related applications.

Dan Li

Dan Li received his B. Sc. from Sun Yat-Sen University in 1984 and then worked at Shantou University. He pursued his Ph. D. at The University of Hong Kong with Professor Chi-Ming Che during 1988–1993. He then returned to Shantou University and became Professor in 2001. He moved to Jinan University in Guangzhou in 2016. He was a recipient of the National Science Fund for Distinguished Young Scholars of China in 2008 and a Fellow of The Royal Society of Chemistry (FRSC) in 2014. He has been working in the field of supramolecular coordination chemistry and focuses his research interest on the design and fabrication of supramolecular coordination assemblies and their functions including photoluminescence, porosity, and chirality.

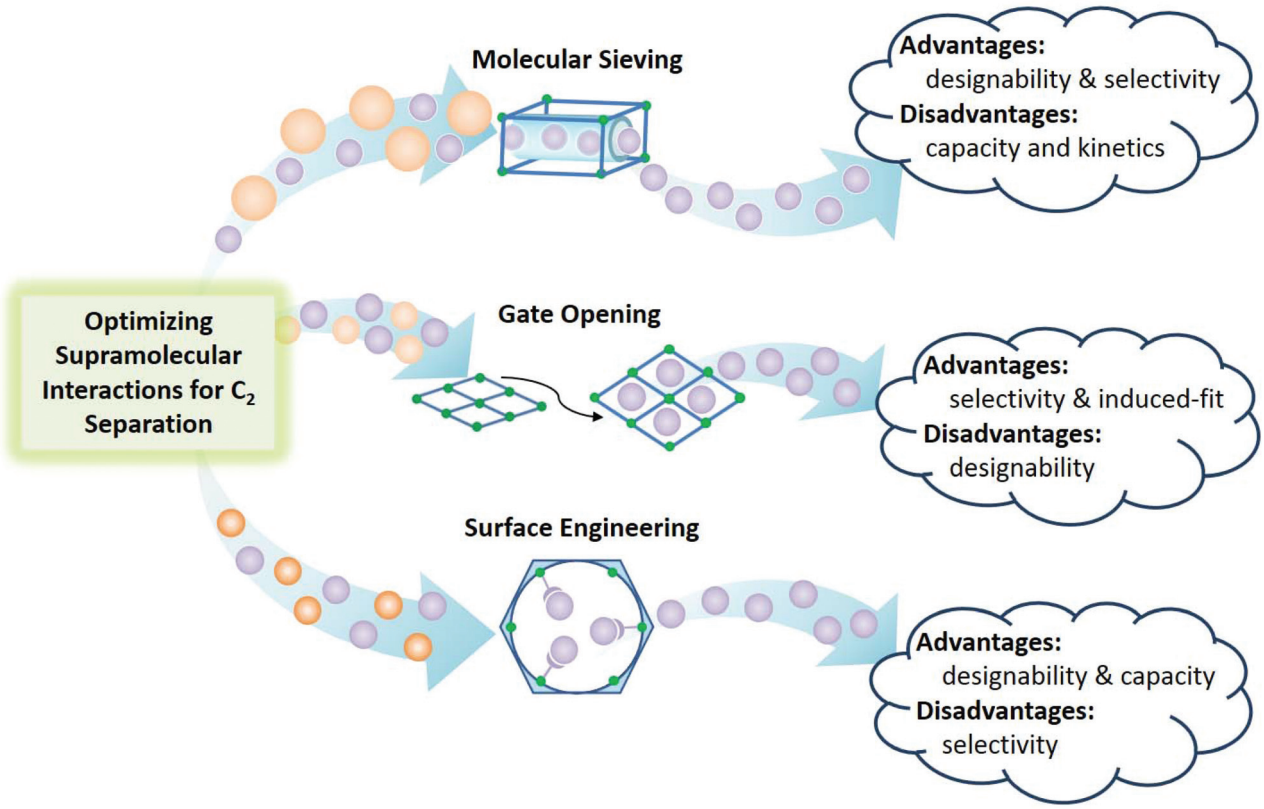

Fig. 1 Illustration of the three most frequently used design strategies of MOF materials for C_2 separation hinged upon supramolecular interactions: molecular sieving, gate opening, and surface engineering.

A pillar-layered MOF exemplifies MOF's structural designability, as the layer structure is usually not affected by the change of pillars; thus, different apertures and functions can be obtained through a judicious selection of pillars of different lengths and/or bearing different functional groups.[29] In 2011, Chen *et al.* reported two microporous pillar-layered MOFs for the selective separation of C_2H_2/C_2H_4.[30] Two-dimensional (2D) 3^6 tessellated $Zn_3(BDC)_3$ and $Zn_3(CDC)_3$ sheets were first formed by linking $Zn_3(COO)_6$ secondary building blocks with BDC (1,4-benzenedicarboxylate) and CDC (1,4-cyclohexanedicarboxylate) ligands, respectively. These two sheets were further expanded by using the chiral metalloligand Cu(SalPyCy) to form two pillar-layered mixed-metal–organic frameworks (M'MOFs), M'MOF-2 and M'MOF-3. The selectivity of M'MOF-3a ('a' stands for 'activated') for C_2H_2/C_2H_4 separation was calculated to be 25.5, which is significantly higher than that of M'MOF-2a (1.6). The jump in selectivity contributed to the slightly reduced pore size of M'MOF-3 (3.4×4.8 Å^2), which falls right between the kinetic sizes of C_2H_2 and C_2H_4. Using the same strategy, Cai *et al.* reported another pillar-layered M'MOF,[31] MECS-5, which not only inherited the sieving effect of the M'MOF series but also showed a high C_2H_2 adsorption capacity (3.85 mmol g^{-1}, 86.2 cm^3 g^{-1}, 298 K and 1 bar), demonstrating that the pillar-layered synthetic strategy is an effective approach to tune the pore sizes and shapes, achieving both high adsorption capacity and selectivity. Although many pillar-layered MOFs with precisely controlled pore sizes have been reported, they have rarely been employed for industrial purposes probably due to their relatively low porosity and limited stability compared to non-pillared three-dimensional (3D) MOFs.[32] For example, Chen *et al.* reported a dual-functional 3D MOF, UTSA-100,[33] with pore size (3.96 Å) slightly smaller than the kinetic diameter of C_2H_4 (4.2 Å) but larger than that of C_2H_2 (3.3 Å). As a result, UTSA-100a demonstrated not only an excellent sieving effect but also high adsorption capacity for C_2H_2/C_2H_4 separation. Experimental results further confirmed the high efficiency in the removal of trace C_2H_2 from C_2H_2/C_2H_4 mixtures, a challenging industrial separation task (Table 1).

Although of recent origin, MOFs have already been well established in their structural designability through reticular chemistry.[8,34] For example, the same inorganic metal cluster can be connected to organic linkers of different sizes or bearing different functional groups, leading to isoreticular structures with predetermined cavity sizes and functions.[35] A good practice of reticular chemistry is the synthesis of SIFSIX series MOF materials. By using a shorter organic linker of 4,4′-azopyridine (azpy, 9.0 Å) instead of 4,4′-dipyridylacetylene (dpa, 9.6 Å), isoreticular SIFSIX-14-Cu-i (UTSA-200) was synthesized,[36] which has the same dual interpenetrating network

Table 1 Summary of the MOF materials discussed in this paper and their C_2 separation parameters

MOFs	BET surface area ($m^2\ g^{-1}$)	C_2 separation	Adsorption uptake (mmol g^{-1})	Separation selectivity[a]	Temperature and pressure	Design strategies	Ref.
M'MOF-3	110	C_2H_2/C_2H_4	6.56/1.35	25.5	195 K, 1 bar	Molecular sieving	30
MECS-5	—	C_2H_2/C_2H_4	3.85/1.14	12.6	298 K, 1 bar	Molecular sieving	31
UTSA-100	970	C_2H_2/C_2H_4	4.27/1.66	10.72	296 K, 1 bar	Molecular sieving	33
SIFSIX-14-Cu-i (UTSA-200)	612	C_2H_2/C_2H_4	3.65/0.63	6320	298 K, 1 bar	Molecular sieving	36
UTSA-280	331	C_2H_4/C_2H_6	2.5/0.098	>10 000	298 K, 1 bar	Molecular sieving	37
Ni-gallate	424	C_2H_4/C_2H_6	1.97/0.28	16.8	298 K, 1 bar	Molecular sieving	38
Mg-gallate	559	C_2H_4/C_2H_6	3.03/0.26	37.3	298 K, 1 bar	Molecular sieving	38
Co-gallate	475	C_2H_4/C_2H_6	3.37/0.31	52	298 K, 1 bar	Molecular sieving	38
JNU-2	1219	C_2H_6/C_2H_4	4.19/3.6	1.6	298 K, 1 bar	Molecular sieving	39
ZIF-7	230	C_2H_6/C_2H_4	2.24/2.2	1.75[b]	298 K, 1 bar	Gate opening	41
RPM3-Zn	328	C_2H_2/C_2H_4	2.14/0.89	—	298 K, 1 bar	Gate opening	42
RPM3-Zn	328	C_2H_6/C_2H_4	1.56/0.89	—	298 K, 1 bar	Gate opening	42
UTSA-300	311	C_2H_2/C_2H_4	3. 08/0.04	$>10^4$	298 K, 1 bar	Gate opening	43
NCU-100	358	C_2H_2/C_2H_4	4.57/0.32	7291	298 K, 1 bar	Gate opening	44
[Co(VTTF)]	—	C_2H_4/C_2H_6	1.36/0.11	—	273 K, 1 bar	Gate opening	45
Fe-MOF-74	1350	C_2H_4/C_2H_6	6.28/5.10	13.6	298 K, 1 bar	Surface engineering	63
$Fe_2(O_2)$(dobdc)	1073	C_2H_6/C_2H_4	3.32/2.53	4.4	298 K, 1 bar	Surface engineering	64
MIL-101-Cr-SO_3Ag	1374	C_2H_4/C_2H_6	3.26/1.47	9.7	296 K, 1 bar	Surface engineering	66
NOTT-300	1370	C_2H_4/C_2H_6	4.28/0.85	48.7	293 K, 1 bar	Surface engineering	67
SIFSIX-2-Cu-i	503	C_2H_2/C_2H_4	4.02/2.19	44.54	298 K, 1 bar	Surface engineering	68
MAF-49	—	C_2H_6/C_2H_4	1.73/1.7	9	316 K, 1 bar	Surface engineering	69
ZJU-120	1597	C_2H_6/C_2H_4	4.91/3.93	2.74[b]	296 K, 1 bar	Surface engineering	74

[a] IAST selectivity for a 1/99 mixture. [b] IAST selectivity for an equimolar mixture.

structure as SIFSIX-2-Cu-i, but a reduced pore size. The superfine 1D channel (3.4 Å) in UTSA-200a (Fig. 2a–d) renders it an ideal molecular sieve for C_2H_2 with an IAST selectivity of over 6000 for a C_2H_2/C_2H_4 (1/99, v/v) mixture at 1 bar and 298 K (Fig. 2f). High-resolution neutron powder diffraction data were collected for C_2D_2-loaded samples of UTSA-200a, suggesting each adsorbed C_2H_2 molecule interacting with two SIF_6^{2-} anions from different nets through C–H···F H-bonding (Fig. 2b). In contrast, computational results indicated that when C_2H_4 molecules were loaded into the pore, the C_2H_4 molecules would have inevitable space overlapping with the pore walls (Fig. 2c). The results are consistent with a high adsorption capacity of C_2H_2 and almost no adsorption of C_2H_4 in UTSA-200a (Fig. 2e).

Compared to C_2H_2/C_2H_4, the molecular sieving separation of C_2H_4/C_2H_6 appears to be more challenging because of their closer molecular sizes (C_2H_4: 4.163 Å; C_2H_6: 4.443 Å). In 2018, Chen *et al.* reported an ultra-microporous MOF [$Ca(C_4O_4)(H_2O)$] (UTSA-280 ⊃ H_2O), synthesized with calcium nitrate and squaric acid.[37] After the removal of guest molecules, 1D cylindrical channels were obtained with aperture sizes of 3.2 × 4.5 $Å^2$ and 3.8 × 3.8 $Å^2$. The cross-sectional areas of these apertures are roughly the same, about 14.4 $Å^2$ (Fig. 3a), which is larger than the minimum cross-sectional area of C_2H_4 (13.7 $Å^2$), but smaller than that of C_2H_6 (15.5 $Å^2$), indicating a good sieving potential for C_2H_4/C_2H_6 separation (Fig. 3b and c). Single-crystal X-ray diffraction (SCXRD) experiments were carried out on C_2H_4-loaded samples to locate the C_2H_4 molecules inside UTSA-280, and it was found that C_2H_4 molecules interacted not only with ligands but also with coordinated water molecules through C–H···O hydrogen bonds, π···π stack-

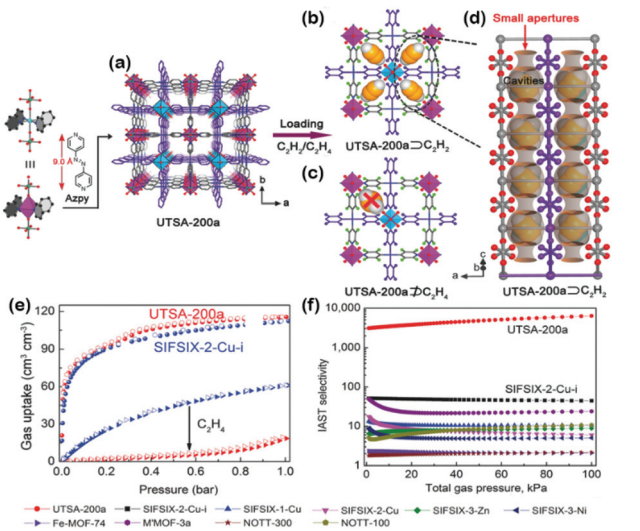

Fig. 2 (a) The channel structure of UTSA-200a reveals a pore size of ≈3.4 Å. (b) DFT-D-calculated C_2H_2 adsorption models in UTSA-200a, revealing that this pore size enables the passage of C_2H_2 molecules. (c) Simulated C_2H_4 adsorption in UTSA-200a indicating that the C_2H_4 molecule is too large to pass through the pores. (d) Schematic illustration of ideal molecular sieves based on the structure of UTSA-200a ⊃ C_2H_2, in which larger cavities suitable for strongly binding C_2H_2 molecules are interconnected by narrow apertures that serve as sieves for C_2H_2. (e) Adsorption isotherms of C_2H_2 (circles) and C_2H_4 (triangles) for UTSA-200a and SIFSIX-2-Cu-i at 298 K. (f) Comparison of the IAST selectivity of UTSA-200a *versus* the other best-performing materials. (Reprinted with permissions from ref. 36; copyright 2017, Wiley-VCH Verlag GmbH & Co. KGaA, Weinheim).

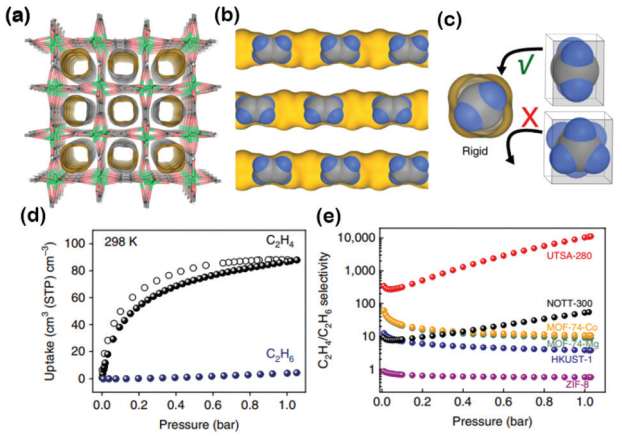

Fig. 3 (a) The crystal structure of guest-free UTSA-280 determined from single-crystal X-ray diffraction, showing one-dimensional channels viewed along the [001] direction. (b) Top and side views of the packing diagram of the C_2H_4 adsorbed structure. (c) Schematic diagram of the size/shape sieving based on the minimum cross-sectional areas of C_2H_4 and C_2H_6 molecules. (d) Single-component sorption isotherms of C_2H_4 (black), C_2H_6 (indigo) at 298 K for UTSA-280. (e) Qualitative comparison of IAST adsorption selectivities of different MOFs for an equimolar C_2H_4/C_2H_6 mixture at 298 K. (Reprinted with permissions from ref. 37; copyright 2018, Springer Nature).

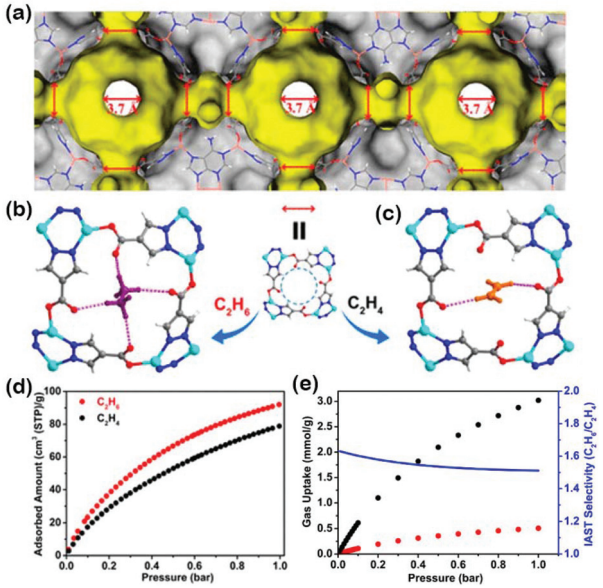

Fig. 4 (a) Schematic illustration of the multistage apertures in JNU-2 (Connolly surface). (b and c) Comparison of the host–guest interactions of C_2H_6 and C_2H_4 with JNU-2 at the aperture by DFT calculations. (d) C_2H_6 and C_2H_4 single component adsorption isotherms of JNU-2 at 298 K. (e) Predicted mixture adsorption isotherms and predicted IAST selectivity of JNU-2 for a 10 : 90 C_2H_6/C_2H_4 mixture at 298 K. (Reprinted with permissions from ref. 39; copyright 2019, American Chemical Society).

ing, and van der Waals interactions (C–H···π). Overall, the C_2H_4 uptake in UTSA-280 can reach as much as 2.5 mmol g^{-1} at 298 K and 1 bar, while the C_2H_6 uptake (0.098 mmol g^{-1}) is negligible under the same conditions (Fig. 3d). In addition, the IAST selectivity for an equimolar C_2H_4/C_2H_6 mixture can reach up to 10 000 at 298 K and 1 bar (Fig. 3e), which is much higher than other MOFs reported so far. In a separated work, Chen *et al.* reported a series of gallate-based MOFs with pores well suited for the molecular sieving separation of C_2H_4/C_2H_6.[38] The gallate-based MOFs [$M(C_7O_5H_4)\cdot 2H_2O$, M = Ni, Mg, Co] consist of 3D interconnected channels (3.47 × 4.85, 3.56 × 4.84, and 3.69 × 4.95 $Å^2$, for Ni, Mg, and Co-gallate, respectively). These values are all slightly larger than the minimum cross-section size of the C_2H_4 molecule (3.28 × 4.18 $Å^2$) but significantly smaller than that of C_2H_6 (3.81 × 4.08 $Å^2$), suggesting that C_2H_6 molecules can be excluded from the pore while C_2H_4 molecules can enter inside, which was further confirmed by gas adsorption data and breakthrough experiment results.

Although exceptionally high selectivity could be reached, the size-based molecular sieving of C_2H_4 from C_2H_4/C_2H_6 mixtures is not an ideal separation strategy in terms of energy efficiency due to the necessity of further desorption to produce C_2H_4. Compared with MOFs that preferentially adsorb C_2H_4, the separation efficiency of MOFs preferentially adsorbing C_2H_6 will be significantly improved, because high-purity C_2H_4 can be directly obtained through a single adsorption step, simplifying the separation process, and reducing the energy penalty simultaneously. Li *et al.* reported a C_2H_6-selective MOF (JNU-2) with a rare xae topological structure. Its cage-like cavities were interconnected by limiting apertures of about 3.7 Å (Fig. 4a),[39] which is in the domain of the kinetic diameters of C_2H_4 and C_2H_6 molecules. The surface on the aperture of JNU-2 is equipped with high-density oxygen atoms, and the four oxygen atoms preferentially interact with C_2H_6 over C_2H_4 through multiple C–H···O hydrogen bonds (Fig. 4b and c), resulting in a high selectivity of C_2H_6 over C_2H_4 and C_2H_6 adsorption capacity of 4.19 mmol g^{-1} (92.0 cm^3 g^{-1}) at 298 K and 1 bar (Fig. 4d and e). Due to the interconnecting apertures, the dumbbell-shaped channels function as multi-level sieves for C_2H_6 molecules to diffuse in and out of the framework, leading to an increased selectivity preferentially for C_2H_6. Thus, JNU-2 can be viewed as an interaction-induced molecular sieve for C_2H_6 and is potentially useful for the energy efficiency separation of C_2H_4/C_2H_6 mixtures.

The molecular sieving strategy has been frequently applied in the design and synthesis of MOF materials for hydrocarbon separation. MOFs with suitable pore apertures can effectively separate molecules of different kinetic diameters, which works particularly well for small-sized and rigid ones such as C_2.[21] Nevertheless, appropriate surface engineering on the aperture could induce strong host–guest interaction with molecules of matching physicochemical properties (not necessarily the small-sized ones); thus, it could be rendered in an interaction-induced molecular sieve. Considering their small difference in kinetic diameters (C_2H_2, C_2H_4, and C_2H_6: 3.3, 4.163, and 4.443 Å, respectively), the development of MOF materials with a molecular sieving effect on C_2 is challenging, but exceptionally high selectivity has been proved if well designed. Overall,

MOFs with a molecular sieving effect provide promising energy-saving alternatives to solve important industrial gas separation problems.

Gate opening

Besides structural designability, framework flexibility is another important property of some MOFs, which could also have a profound effect on gas adsorption. Compared to rigid MOFs, flexible MOFs are the ones that undergo reversible framework transformation in response to external stimuli. One particular framework flexibility is the gate opening most commonly observed upon increasing gas pressure. MOFs with gate-opening behaviour can be applied in adsorptive separations, providing that gas separation induces gate opening at different pressures. As a result, by a careful control of the partial pressures, such MOF materials will adsorb only the ones having partial pressures that can induce the gate opening. More specifically, the gate-opening effect is similar to the interaction-induced molecular sieving effect, preferentially taking up gas molecules of particular physicochemical properties, not necessarily the small-sized ones.[40] For example, Gascon *et al.* reported a zeolitic imidazolate framework ZIF-7 [41] with preferential adsorption of paraffin over olefin. The interaction between guest molecules and the benzene rings on the ZIF-7 cages strongly affects the adsorption process, inducing gate opening at different threshold pressures. C_2H_6 can penetrate the cage at a lower pressure than C_2H_4, and fit better in the opening form of the ZIF-7 cage. As a result, ZIF-7 exhibits an adsorption selectivity in favour of C_2H_6.

More recently, Chabal *et al.* synthesized a flexible MOF RPM3-Zn with mixed ligands of 4,4′-biphenyl dicarboxylate (bpdc) and 1,2-bipyriylethylene (bpee)[42] (Fig. 5a). The MOF material demonstrated the separation of not only C_2H_2/C_2H_4 but also C_2H_4/C_2H_6 mixtures due to the different gate-opening pressures under different gases (Fig. 5b). Combining Raman spectroscopy and van der Waals density functional (vdW-DF) calculations, it was speculated that the separation capability could be attributed to the H-bonding between the terminal groups of C_2 and the C═O bond of the bpdc ligand. In other words, the H-bonding strength is the dominant effect on the dihedral angle and thus gate-opening (Fig. 5c). The terminal methyl group of C_2H_6 was found to form strong H-bonds, outcompeting the high-density of π-electrons in C_2H_4, while C_2H_2 is much more acidic and forms the strongest H-bonds out of three C_2 (Fig. 5d–f). Overall, the gate-opening pressure was determined for C_2 as follows: $C_2H_2 < C_2H_6 < C_2H_4$ (Fig. 5b), suggesting the potential of employing pressure swing adsorption to separate these three similar-sized molecules.

Using rotatable SiF_6^{2-} as a pillar and flexible 4,4′-dipyridylsulfide (dps) as a ligand, Chen *et al.* designed and synthesized two flexible MOFs, UTSA-300,[43] and NCU-100 (UTSA-300-Cu).[44] UTSA-300 has 2D channels of about 3.3 Å in size, which matches well with the kinetic diameter of C_2H_2. The substitution of zinc(II) with copper(II) resulted in NCU-100 with an expanded pore cavity because of the elongated Cu–F bond (Fig. 6a and b). Both MOF materials exhibit a pore open-close transition upon activation/desolvation, accompanied by the conformation change of the pyridyl ligands and the rotation of SiF_6^{2-} pillars. Strong C–H···F and π–π stacking interactions are found in closed-pore UTSA-300a and NCU-100a, resulting in a shrinkage of these structures. Thus, all apertures are blocked in the closed-pore UTSA-300a and NCU-100a (Fig. 6d), which only allows C_2H_2 to penetrate with a complete exclusion of C_2H_4 and CO_2 under ambient conditions. Further studies reveal that the C_2H_2 molecule primarily binds to two F atoms in a head-on orientation, breaking the original internetwork H-bonds. After C_2H_2 adsorption, UTSA-300a and NCU-100a expand from the closed-pore to their open-pore structure (UTSA-300a ⊃ C_2H_2 and NCU-100a ⊃ C_2H_2) (Fig. 6e). NCU-100a has a higher C_2H_2 absorption capacity (4.57 mmol g^{-1}) than UTSA-300a (3.08 mmol g^{-1}) at 298 K and 1.0 bar (Fig. 6f), likely due to the extension of the internal cavities and stronger C_2H_2 affinity. Notably, the IAST selectivity of NCU-100a for C_2H_2/C_2H_4 (1/99, v/v) was calculated to be 7291 at 1.0 bar and 298 K, which is more than two orders of magnitude higher than that of UTSA-300a and also higher than those of other state-of-the-art materials in C_2H_2/C_2H_4 separation (Fig. 6g).

In addition, Kitagawa *et al.* reported a soft porous crystal possessing exclusive gate opening for C_2H_4 by making use of the reversible hemilabile cross-linking in its framework.[45] The as-synthesized Co-based porous coordination polymer [Co

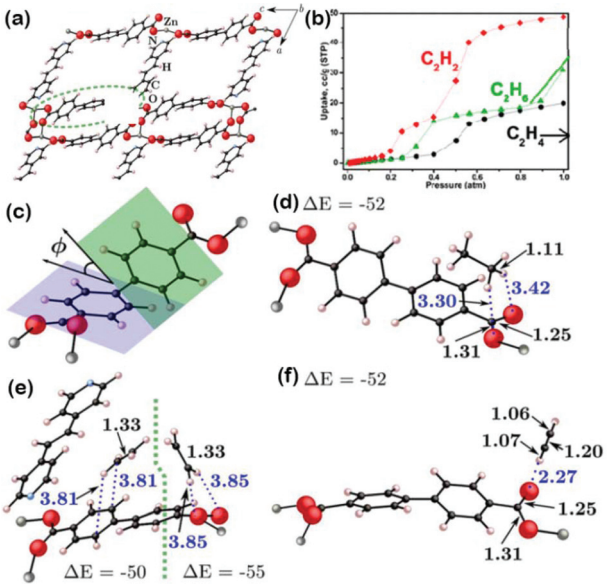

Fig. 5 (a) Side view of the RPM3-Zn structure. (b) Adsorption–desorption isotherms of C_2H_2 (red), C_2H_6 (green), C_2H_4 (black) in RPM3-Zn at 298 K plotted as a function of relative pressure. (c) Dihedral angle in the bpdc ligand. (d, e, f) Local fragments showing interactions with C_2H_6, C_2H_4, and C_2H_2 adsorbed in RPM3-Zn, respectively. (Reprinted with permissions from ref. 42; copyright 2012, American Chemical Society).

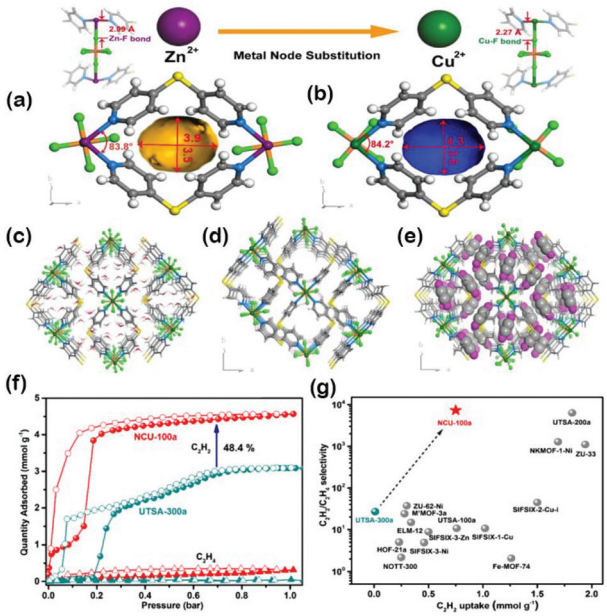

Fig. 6 (a) Isoreticular structure of the zinc analogue UTSA-300 and (b) copper analogue NCU-100. (c and d) Perspective views of cage units in NCU-100 and NCU-100a, showing the tilting of the pyridine ring and C–H···F interactions upon desolvation. (e) Crystal structure and simplified diagram of NCU-100a ⊃ C_2H_2. (f) Adsorption isotherms of C_2H_2 and C_2H_4 on NCU-100a and UTSA-300a in the pressure regions of 0–1.05 bar at 298 K. (g) Comparison of C_2H_2 uptake at 0.01 bar and 1/99 C_2H_2/C_2H_4 selectivity in NCU-100a (triangles), UTSA-300a (circles) and other representative MOFs. (Reprinted with permissions from ref. 44; copyright 2020, American Chemical Society).

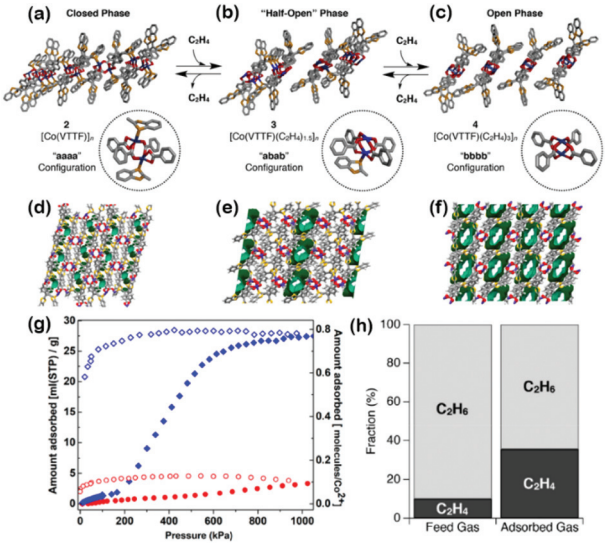

Fig. 7 Structural transformations of the Co(VTTF) PCP. Crystal structures of (a) **2** (evacuated phase), (b) **3** ("half-open" phase), and (c) **4** (fully open phase). (d–f) Void spaces in structures **2**, **3**, and **4**, respectively. The void spaces were visualized using the Mercury CSD 3.5.1 software with a probe radius of 1.2 Å. (g) Adsorption/desorption isotherms for **2** with C_2H_4 (blue) and C_2H_6 (red) at 283 K to 1 MPa. (h) Schematic presentations of ethylene and ethane fractions in the feed and adsorbed gases with a feed gas consisting of a C_2H_4/C_2H_6 mixture in a 10 : 90 ratio. (Reprinted with permissions from ref. 45; copyright 2017, American Chemical Society).

(VTTF)] (VTTF = 2,2′-[1,2-bis(4-benzoicacid)-1,2-ethanediylidene]bis-1,3-benzodithiole) was a 1D chain that stacks together *via* intermolecular C–H···π interactions. Upon activation, the formation of Co–S bonds between the Co and S atoms on the VTTF ligand crosslinked 1D chains into an overall nonporous 3D framework. It was found that C_2H_4 molecules with π-coordinating ability were able to "unlock" the closed structure by breaking the Co–S bond and trigger a transition from a nonporous to a porous single crystal, opening additional void space for C_2H_4 adsorption. In contrast to C_2H_4, however, C_2H_6 was unable to open the nonporous phase and its adsorption can be ignored (Fig. 7g). More interestingly, the gate-opening structural transformation event follows a two-step process, that is, forming a "half-open" intermediate state, followed by a full open phase (Fig. 7a–f). Each state in this two-step gate-opening process was individually characterized by SCXRD analysis, which revealed that the non-porous-to-porous single-crystal-to-single-crystal (SCSC) transformation is indeed triggered by C_2H_4 molecules disrupting the Co–S bonds.

Flexible MOFs exhibit high adsorption selectivity due to different gate-opening pressures of gas molecules, which are dependent on their individual physicochemical properties; thus, the underlying mechanism is similar to the interaction-induced molecular sieving effect. More interestingly, MOFs with limited flexibility could exert a synergistic effect on gas separation by combining size-based molecular sieving and gate-opening mechanisms in the same MOF materials.[46,47] For example, the material MAF-41 demonstrated the adsorption of styrene by completely excluding not only large ethylbenzene molecules (size-exclusion) but also small toluene/benzene molecules (insufficient adsorption energy to open the cavity), realizing a unique intermediate-sized molecular sieving (iSMS) effect.[48] In a word, the gate-opening pressure of adsorption is determined by using the molecular size of the guest and its binding affinity, and further exploration in this direction could lead to interesting adsorption behaviour which might be applicable in situations of difficult industrial hydrocarbon separation.

Surface engineering

In addition to molecular sieving and gate opening, surface engineering has also been frequently employed to achieve selective adsorption.[49] MOFs with large pores usually exhibit no sieving effect and therefore low adsorption selectivity, but large pore volumes are beneficial for adsorption capacity.[50] Fortunately, due to structural designability, various functional groups can be introduced into MOF channels and cavities, amplifying the binding affinity toward different guest molecules and thus improving adsorption selectivity.[51,52] For instance, open metal sites (OMSs) have a special binding ability for unsaturated hydrocarbons by forming

π-complexation, resulting in preferential adsorption of unsaturated hydrocarbons. Moreover, the host–guest interactions can be further tuned and differentiated by introducing appropriate functional groups on the surface.[53,54]

OMSs are coordinatively unsaturated metal ions that function as Lewis acids, and it has been an active research field for preferentially binding and activating specific molecules in recent years.[55–58] Of the multitude of MOF structures reported over the past two decades, M-MOF-74 (M = Fe, Co, Ni, Cu, Zn, and Mg) are probably the most studied isostructural series that have a high density of OMSs.[51,59–62] Although M-MOF-74s do not have the sieving effect because of their large pores (11 Å), their OMSs on the surface preferentially interact with unsaturated hydrocarbons over their saturated counterparts; therefore, they can be potentially applied in C_2H_4/C_2H_6 and C_3H_6/C_3H_8 separations. For example, they can be applied on the hexagonal channels of Fe-MOF-74 (Fe_2(dobdc)) lined with square pyramid-shaped Fe^{2+} cations (Fig. 8a), and each cation has an open coordination site pointing towards the channel.[63] Fe-MOF-74 has a strong affinity for unsaturated hydrocarbons, such as C_2H_2, C_2H_4, and C_3H_6, with Fe-C distances lying in the range of 2.42(2) to 2.60(2) Å (Fig. 8b). As a result, Fe-MOF-74 was demonstrated in the separation of not only C_2H_4/C_2H_6 and C_3H_6/C_3H_8 mixtures but also an equimolar four-component mixture of $CH_4/C_2H_6/C_2H_4/C_2H_2$ (Fig. 8c and d). Interestingly, *via* the addition of O_2 to iron(II) on Fe_2(dobdc), Bloch *et al.* introduced iron(III) peroxo sites on the pore surface.[64] The obtained $Fe_2(O_2)$(dobdc) exhibits preferential binding with C_2H_6 over C_2H_4. Neutron powder diffraction studies indicated that the Fe(III)-peroxo sites engage in close contacts with one of the methyl groups of the adsorbed C_2H_6 molecules. Therefore, the uptake capacity of C_2H_6 (3.32 mmol g^{-1}, 74.3 cm^3 g^{-1}) in $Fe_2(O_2)$(dobdc) is higher than that of C_2H_4, leading to an unprecedented high C_2H_6/C_2H_4 separation selectivity (4.4) for a 1 : 1 mixture at 298 K and 1 bar. However, like many other MOFs with OMSs, both Fe_2(dobdc) and $Fe_2(O_2)$(dobdc) are air-sensitive, and therefore, their performance under humid conditions is not discussed.

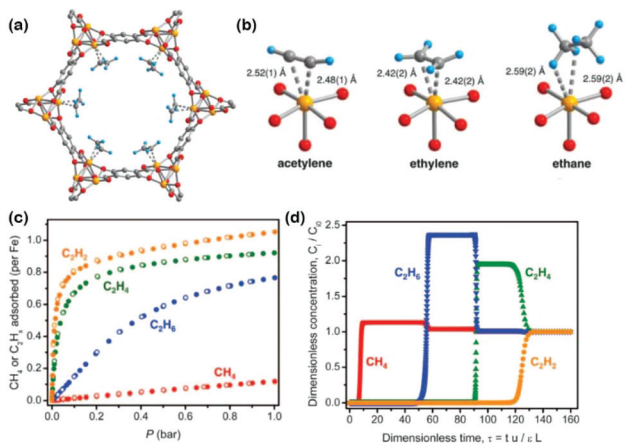

Fig. 8 (a) A portion of the solid-state structure of Fe_2(dobdc)·$2C_2D_4$ as determined by analysis of neutron powder diffraction data and shows an ethylene molecule bound to the open coordination site at each iron(II) center. (b) Fe_2(dobdc) with acetylene, ethylene, ethane. (c) Gas adsorption isotherms for methane, ethane, ethylene, and acetylene in Fe_2(dobdc) at 318 K. (d) Calculated methane (red), ethane (blue), ethylene (green), and acetylene (orange) breakthrough curves for an equimolar mixture of the gases at 1 bar flowing through a fixed bed of Fe_2(dobdc) at 318 K. (Reprinted with permissions from ref. 63; copyright 2012, American Association for the Advancement of Science).

The Ag(I) ion is known for forming silver–olefin complexes in organometallic chemistry due to the interaction between the d orbital of Ag(I) and the π* orbital of the olefin double bond.[65] Inspired by its ability to form π-complexation, Ma *et al.* designed and synthesized MIL-101-Cr-SO_3Ag *via* the Ag(I) ion exchange of sulphonic acid-functionalized MIL-101-Cr (MIL-101-Cr-SO_3H).[66] Compared with pristine MIL-101-Cr-SO_3H, the C_2H_4 adsorption capacity of MIL-101-Cr-SO_3Ag significantly increased from 1.65 mmol g^{-1} (37 cm^3 g^{-1}) to 2.81 mmol g^{-1} (63 cm^3 g^{-1}) at 318 K, and the adsorption selectivity also increased from 1.2 to 9.7, demonstrating the introduction of Ag(I) as an efficient approach for C_2H_4/C_2H_6 separation. The high C_2H_4/C_2H_6 adsorption selectivity of MIL-101-Cr-SO_3Ag was mainly attributed to the π-complexation between Ag(I) ions and the C_2H_4 molecules. In addition, the possible cooperative contribution from Cr(III) as the second OMSs to further enhancing the C_2H_4/C_2H_6 adsorption selectivity was discussed by comparing the selectivity with PAF-1-SO_3Ag.

In addition to OMSs, Lewis basic/acidic sites can also interact with unsaturated hydrocarbons, resulting in equally significant host–guest interactions. For example, Yang *et al.* reported a hydroxyl-functionalized Al-MOF, NOTT-300,[67] which can form multiple supramolecular interactions with unsaturated hydrocarbons. Thus, NOTT-300 exhibited a C_2H_4/C_2H_6 selectivity of 48.7, which was much higher than that of Fe-MOF-74 (13.6), the one with a high density of OMSs. Similarly, the electronegative F atoms on the SiF_6^{2-} pillars of SIFSIX materials were found to interact with hydrocarbons to form C–H···F H-bonds, especially with more acidic C_2H_2. As a result, the SIFSIX materials demonstrated preferential binding with C_2H_2 molecules and excellent C_2H_2 adsorption performance. Particularly, SIFSIX-2-Cu-i could significantly minimize the trade-off between adsorption capacity and C_2H_2/C_2H_4 selectivity, showing a high C_2H_2/C_2H_4 selectivity (39.7 to 44.8) and C_2H_2 absorption capacity (2.1 mmol g^{-1}), realizing an excellent separation performance for C_2H_2/C_2H_4 mixtures.[68]

On the other hand, as the polarizability of C_2H_6 is higher than that of C_2H_4 (44.7×10^{25} *vs.* 42.52×10^{25} cm^3), we can design pore cavities to better accommodate C_2H_6 and achieve reverse adsorption selectivity.[39,64,69–73] For example, Zhang *et al.* reported a C_2H_6-selective microporous MOF (MAF-49) with a pore surface decorated with four uncoordinated nitrogen sites, a pair of free amino groups, and a pair of methylene groups.[69] Detailed experimental and computational studies revealed that C_2H_6 can form three strong C–H···N hydrogen bonds and three weak C–H···N electrostatic interactions with C_2H_6 (Fig. 9a), while two less strong C–H···N hydrogen bonds

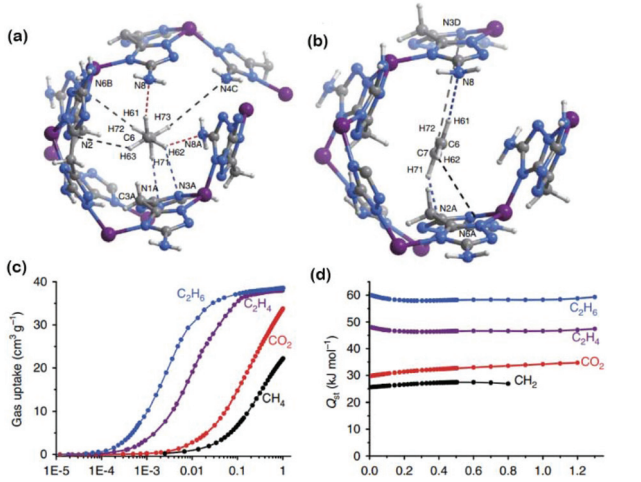

Fig. 9 Preferential adsorption sites for (a) C_2H_6, (b) C_2H_4 in MAF-49 revealed by computational simulations (Zn purple, C dark grey, H light grey, N blue). (c) Gas adsorption isotherms for C_2H_6, C_2H_4, CO_2, and CH_4 in MAF-49 at 316 K. (d) The coverage-dependent C_2H_6, C_2H_4, CO_2 and CH_4 adsorption enthalpy obtained by the Virial method. (Reprinted with permissions from ref. 69; copyright 2015, Springer Nature).

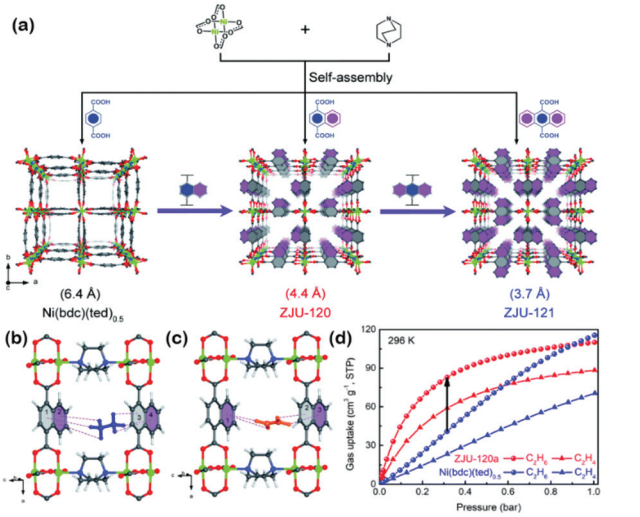

Fig. 10 (a) Structure description of Ni(bdc)(ted)$_{0.5}$, ZJU-120 and ZJU-121, revealing the contracted pore size by introducing aromatic rings in the channels. Comparison of the optimal (b) C_2H_6 and (c) C_2H_4 adsorption sites in ZJU-120a. (d) Gas adsorption isotherms of ZJU-120a and Ni(bdc)(ted)$_{0.5}$ for C_2H_6 and C_2H_4 at 296 K. (Reprinted with permissions from ref. 69; copyright 2020, Royal Society of Chemistry).

and two very weak C–H···N electrostatic interactions were observed for C_2H_4 (Fig. 9b). The binding energies for C_2H_6 and C_2H_4 were calculated to be 56.7 and 45.5 kJ mol^{-1}, respectively (Fig. 9d). As a result, MAF-49 can selectively trap C_2H_6 over C_2H_4 (Fig. 9c), and the adsorption capacity of C_2H_6 is higher than that of C_2H_4, leading to an inverse C_2H_6/C_2H_4 selectivity of 9 at 316 K.

More recently, Li *et al.* reported a controlled synthesis of a family of isomorphic MOFs by altering the carboxylate linker in Ni(bdc)(ted)$_{0.5}$ through reticular chemistry and developed two novel isoreticular MOFs with tuned pore size and rich aromatic rings, Ni(ndc)(ted)$_{0.5}$ and Ni(adc)(ted)$_{0.5}$ (termed ZJU-120 and ZJU-121, respectively) (Fig. 10a).[74] Both MOFs exhibited high adsorption capacity and C_2H_6 selectivity, particularly ZJU-120a, the one with an optimized pore size (4.4 Å). Theoretical computations using first-principles dispersion-corrected density functional theory (DFT-D) revealed that the C_2H_6 molecule interacts with four aromatic rings from two opposite naphthalene rings to form six C–H···π interactions, while C_2H_4 molecules form only four C–H···π interactions with three aromatic rings (Fig. 10b and c). As a result, ZJU-120a demonstrated a high C_2H_6 absorption capacity (4.91 mmol g^{-1}, 110 cm^3 g^{-1} at 1 bar and 296 K) and C_2H_6/C_2H_4 selectivity (2.74), which is superior to original Ni(bdc)(ted)$_{0.5}$ (Fig. 10d).

Although a large pore volume would be beneficial for high adsorption capacity, MOFs with large pores usually possess no sieving effect and therefore usually negligible selectivity. For hydrocarbon separation, surface engineering with OMSs and/or other functional groups can be employed to increase the interaction potential between the host and guest, leading to selective binding towards gas molecules by their difference in polarizability, dipole moment, or quadrupole moment, *etc.* Nevertheless, it is worth pointing out that surface functionalization could substantially compromise the surface area, resulting in a high selectivity at the expense of absorption capacity. Thus, appropriate surface engineering is the key to striking a balance between adsorption capacity and selectivity to cater for different scenarios in hydrocarbon separation.

Conclusions and perspectives

In this review, we extrapolated three major strategies, namely molecular sieving, gate opening, and surface engineering, in the design and synthesis of MOFs for C_2 hydrocarbon separation according to their corresponding supramolecular interactions. The advantages and disadvantages of each of these strategies were highlighted and discussed. Molecular sieving can effectively separate molecules with different kinetic diameters by excluding the large-sized ones, significantly improving the separation selectivity. However, the difference in the kinetic diameters of C_2 hydrocarbons is relatively small, which dictates the MOF structures with meticulously controlled pore apertures, making the design of such MOF materials challenging. On the other hand, a small pore aperture could be translated into a sieving effect and could improve adsorption selectivity, but it could also limit diffusion kinetics and adsorption capacity. The gate-opening effect of flexible MOFs is, in a sense, similar to the interaction-induced molecular sieving effect and could also achieve high adsorption selectivity. Flexible MOFs can self-adapt to accommodate guest molecules of preferred sizes and physicochemical properties, and even exhibit induced-fit behavior like an enzyme,[75] so that the guests can fit more tightly, resulting in increased interaction between the host and guest.[76,77] However, the design and syn-

thesis of flexible MOFs is relatively difficult because of the uncertainty of the self-assembly process and other uncontrollable factors.[78] For MOFs with large pores, on the one hand, they have appreciable space potentially for high adsorption capacity; on the other hand, they exhibit no sieving effect, and therefore usually low adsorption selectivity. Thus, surface engineering is necessary for the MOFs to enhance the adsorption capacity particularly for the target molecule, and improve the adsorption selectivity.

At present, the balance between adsorption selectivity and capacity is still a key issue in adsorptive separation. One viable approach to tackle this issue is to integrate supramolecular interactions in a single MOF system. For example, we reported a stable flexible MOF (JNU-1) with a high density of OMSs,[77] and it showed induced-fit behavior for C_2H_2 through a cooperative action with OMSs, resulting in an enhanced C_2H_2 binding affinity. Moreover, we reported a stable rigid MOF (JNU-2),[39] in which large and small pores were combined through tailored apertures. The apertures function as sieving sites for C_2H_6, while the inner cavities provide space for large adsorption. Similarly, Bu *et al.* proposed an ultra-microporous building unit (UBU) strategy to create hierarchical bi-porous features that can work together to enhance separation performance.[79] Such a structure layout represents a feasible approach to balance the adsorption capacity and selectivity of C_2H_6. In addition, Bu and Feng groups developed a pore space partition (PSP) strategy,[80–83] in which the large pore space can be rationally divided to achieve better gas separation and purification.[84]

Impressively, some MOF materials have demonstrated effective separation from the gas mixtures of more than two components.[59,63,85–87] For example, Lu and Zhou groups reported a MOF (TJT-100) that can efficiently purify C_2H_4 from a ternary mixture of $C_2H_2/C_2H_4/C_2H_6$ (0.5/99/0.5).[88] The uncoordinated carboxylic acid oxygen atoms and coordinated water molecules positioning on the microporous surface of TJT-100 facilitate the formation of multiple electrostatic interactions with the C–H bonds of C_2H_6 and C_2H_2, resulting in the direct production of C_2H_4 with purity greater than 99.997% from a ternary mixture by a single-breakthrough operation. In addition, Chen *et al.* developed a synergistic sorbent separation technology (SSST),[89] in which several adsorbents with good adsorption selectivity for different gases were used to fill the packed bed. Specifically, they used TIFSIX-2-Cu-i for the selective capture of C_2H_2, Zn-atz-ipa for C_2H_6, and SiF_6-3-Ni for CO_2, to produce polymer-grade C_2H_4 in one step from a ternary ($C_2H_2/C_2H_4/C_2H_6$) or quaternary ($CO_2/C_2H_2/C_2H_4/C_2H_6$) gas mixture.

In summary, MOFs have demonstrated great potential and unique advantages in adsorptive separation. On the one hand, we can control pore size/shape and flexibility to match the target molecule. On the other hand, we can introduce strong binding sites on the surface to further enhance the interaction with the target molecule. The successful implementation of integrating these supramolecular interactions could realize the balance between adsorption capacity and selectivity. Furthermore, MOFs' crystalline nature allows the determination of the precise location of the adsorbed molecules through advanced X-ray diffraction techniques and host–guest interactions. A combination of experimental and computational approaches provides an understanding of the adsorption mechanism in-depth and adsorption/desorption dynamics at the molecular level, which can be used to guide the future design of MOF materials. In addition, MOF-based membranes are increasingly gaining momentum due to their structural and chemical versatility, which may broaden their application prospects in hydrocarbon separation.[90–92] Despite all the promising results in adsorption capacity and selectivity, the practical application of MOFs for C_2 hydrocarbon separation is yet to come. Their separation performance under humid conditions could still be easily compromised, because water vapor can easily outcompete unsaturated hydrocarbons for binding sites, resulting in significantly reduced separation performance.[93,94] The future direction in hydrocarbon separation should be focusing on its economic viability, more specifically, developing low-cost synthetic methods for stable MOFs with highly efficient separation performance even under humid conditions.

Conflicts of interest

There are no conflicts to declare.

Acknowledgements

The authors would like to thank the support provided by the National Natural Science Foundation of China (No. 21731002 and 21975104), the Guangdong Major Project of Basic and Applied Research (no. 2019B030302009), and the Guangdong Basic and Applied Basic Research Foundation (no. 2020A1515011005).

Notes and references

1 J. Li, R. J. Kuppler and H. Zhou, *Chem. Soc. Rev.*, 2009, **38**, 1477–1504.
2 A. Van Miltenburg, W. Zhu, F. Kapteijn and J. A. Moulijn, *Chem. Eng. Res. Des.*, 2006, **84**, 350–354.
3 D. S. Sholl and R. P. Lively, *Nature*, 2016, **532**, 435–437.
4 G. Narin, V. F. D. Martins, M. C. Campo, A. M. Ribeiro, A. F. P. Ferreira, J. C. Santos, K. Schumann and A. E. Rodrigues, *Sep. Purif. Technol.*, 2014, **133**, 452–475.
5 J. Pei, K. Shao, L. Zhang, H. Wen, B. Li and G. Qian, *Top. Curr. Chem.*, 2019, **377**, 1–34.
6 B. Li, H. M. Wen, Y. Cui, W. Zhou, G. Qian and B. Chen, *Adv. Mater.*, 2016, **28**, 8819–8860.
7 W. Lu, Z. Wei, Z. Gu, T. Liu, J. Park, J. Park, J. Tian, M. Zhang, Q. Zhang and T. Gentle, *Chem. Soc. Rev.*, 2014, **43**, 5561–5593.
8 O. M. Yaghi, *J. Am. Chem. Soc.*, 2016, **138**, 15507–15509.

9 V. Guillerm, D. Kim, J. F. Eubank, R. Luebke, X. Liu, K. Adil, M. S. Lah and M. Eddaoudi, *Chem. Soc. Rev.*, 2014, **43**, 6141–6172.
10 B. Li and B. Chen, *Chem*, 2016, **1**, 669–671.
11 Y. Yan, S. Yang, A. J. Blake and M. Schroder, *Acc. Chem. Res.*, 2014, **47**, 296–307.
12 N. Stock and S. Biswas, *Chem. Rev.*, 2012, **112**, 933–969.
13 H. M. Wen, B. Li, L. Li, R. Lin, W. Zhou, G. Qian and B. Chen, *Adv. Mater.*, 2018, **30**, 1704792.
14 H. Deng, S. Grunder, K. E. Cordova, C. Valente, H. Furukawa, M. Hmadeh, F. Gandara, A. C. Whalley, Z. Liu and S. Asahina, *Science*, 2012, **336**, 1018–1023.
15 L. Zhang, B. Guo, H. He, X. Zhang, Y. Feng, W. Fan, J. Cao, G. Lu, Y. Chen and D. Sun, *Inorg. Chem.*, 2020, **59**, 695–704.
16 B. Li, X. Chen, P. Hu, A. Kirchon, Y. Zhao, J. Pang, T. Zhang and H. Zhou, *ACS Appl. Mater. Interfaces*, 2019, **11**, 8227–8233.
17 P. Cui, P. Wang, Y. Zhao and W. Sun, *Cryst. Growth Des.*, 2019, **19**, 1454–1470.
18 L. Feng, K. Wang, X. Lv, J. A. Powell, T. Yan, J. Willman and H. Zhou, *J. Am. Chem. Soc.*, 2019, **141**, 14524–14529.
19 J. Pang, S. Yuan, J. Qin, C. Lollar, N. Huang, J. Li, Q. Wang, M. Wu, D. Yuan and M. Hong, *J. Am. Chem. Soc.*, 2019, **141**, 3129–3136.
20 S. Yuan, Y. Chen, J. Qin, W. Lu, L. Zou, Q. Zhang, X. Wang, X. Sun and H. Zhou, *J. Am. Chem. Soc.*, 2016, **138**, 8912–8919.
21 K. Adil, Y. Belmabkhout, R. S. Pillai, A. Cadiau, P. M. Bhatt, A. H. Assen, G. Maurin and M. Eddaoudi, *Chem. Soc. Rev.*, 2017, **46**, 3402–3430.
22 S. Yuan, W. Lu, Y. Chen, Q. Zhang, T. Liu, D. Feng, X. Wang, J. Qin and H. Zhou, *J. Am. Chem. Soc.*, 2015, **137**, 3177–3180.
23 P. Z. Moghadam, A. Li, S. Wiggin, A. Tao, A. G. P. Maloney, P. A. Wood, S. C. Ward and D. Fairenjimenez, *Chem. Mater.*, 2017, **29**, 2618–2625.
24 R. Lin, S. Xiang, W. Zhou and B. Chen, *Chem*, 2020, **6**, 337–363.
25 X. Zhao, Y. Wang, D. Li, X. Bu and P. Feng, *Adv. Mater.*, 2018, **30**, 1705189.
26 R. Lin, S. Xiang, H. Xing, W. Zhou and B. Chen, *Coord. Chem. Rev.*, 2017, **378**, 87–103.
27 H. Furukawa, K. E. Cordova, M. Okeeffe and O. M. Yaghi, *Science*, 2013, **341**, 1230444.
28 W. Cui, T. Hu and X. Bu, *Adv. Mater.*, 2020, **32**, 1806445.
29 X. Yan, S. Li, Y. Jiang, M. Hu and Q. Zhai, *Inorg. Chem. Commun.*, 2015, **62**, 107–110.
30 S. Xiang, Z. Zhang, C. G. Zhao, K. Hong, X. Zhao, D. R. Ding, M. H. Xie, C. De Wu, M. C. Das and R. Gill, *Nat. Commun.*, 2011, **2**, 204.
31 X. Hong, Q. Wei, Y. Cai, B. Wu, H. Feng, Y. Yu and R. Dong, *ACS Appl. Mater. Interfaces*, 2017, **9**, 29374–29379.
32 F. ZareKarizi, M. Joharian and A. Morsali, *J. Mater. Chem. A*, 2018, **6**, 19288–19329.
33 T. Hu, H. Wang, B. Li, R. Krishna, H. Wu, W. Zhou, Y. Zhao, Y. Han, X. Wang and W. Zhu, *Nat. Commun.*, 2015, **6**, 7328.
34 R. Lin, S. Xiang, B. Li, Y. Cui, W. Zhou, G. Qian and B. Chen, *Isr. J. Chem.*, 2018, **58**, 949–961.
35 M. Okeeffe, *Chem. Soc. Rev.*, 2009, **38**, 1215–1217.
36 B. Li, X. Cui, D. Onolan, H. M. Wen, M. Jiang, R. Krishna, H. Wu, R. Lin, Y. Chen and D. Yuan, *Adv. Mater.*, 2017, **29**, 1704210.
37 R. Lin, L. Li, H. Zhou, H. Wu, C. He, S. Li, R. Krishna, J. Li, W. Zhou and B. Chen, *Nat. Mater.*, 2018, **17**, 1128–1133.
38 Z. Bao, J. Wang, Z. Zhang, H. Xing, Q. Yang, Y. Yang, H. Wu, R. Krishna, W. Zhou, B. Chen and Q. Ren, *Angew. Chem., Int. Ed.*, 2018, **57**, 16020–16025.
39 H. Zeng, X.-J. Xie, M. Xie, Y.-L. Huang, D. Luo, T. Wang, Y. Zhao, W. Lu and D. Li, *J. Am. Chem. Soc.*, 2019, **141**, 20390–20396.
40 A. Schneemann, V. Bon, I. Schwedler, I. Senkovska, S. Kaskel and R. A. Fischer, *Chem. Soc. Rev.*, 2014, **43**, 6062–6096.
41 C. Gucuyener, J. V. Den Bergh, J. Gascon and F. Kapteijn, *J. Am. Chem. Soc.*, 2010, **132**, 17704–17706.
42 N. Nijem, H. Wu, P. Canepa, A. M. Marti, K. J. Balkus, T. Thonhauser, J. Li and Y. J. Chabal, *J. Am. Chem. Soc.*, 2012, **134**, 15201–15204.
43 R. Lin, L. Li, H. Wu, H. D. Arman, B. Li, R. G. Lin, W. Zhou and B. Chen, *J. Am. Chem. Soc.*, 2017, **139**, 8022–8028.
44 J. Wang, Y. Zhang, P. Zhang, J. Hu, R.-B. Lin, Q. Deng, Z. Zeng, H. Xing, S. Deng and B. Chen, *J. Am. Chem. Soc.*, 2020, **142**, 9744–9751.
45 S. Sen, N. Hosono, J. Zheng, S. Kusaka, R. Matsuda, S. Sakaki and S. Kitagawa, *J. Am. Chem. Soc.*, 2017, **139**, 18313–18321.
46 J. Zhang, H. Zhou, D. Zhou, P. Liao and X. Chen, *Nat. Sci. Rev.*, 2018, **5**, 907–919.
47 X. Yang, H.-L. Zhou, C.-T. He, Z.-W. Mo, J.-W. Ye, X.-M. Chen and J.-P. Zhang, *Research*, 2019, **2019**, 9463719.
48 D. Zhou, P. Chen, C. Wang, S. Wang, Y. Du, H. Yan, Z. Ye, C. He, R. Huang and Z. Mo, *Nat. Mater.*, 2019, **18**, 994–998.
49 B. R. Barnett, M. I. Gonzalez and J. R. Long, *Trends Chem.*, 2019, **1**, 159–171.
50 Z. Zhang, S. Xiang and B. Chen, *CrystEngComm*, 2011, **13**, 5983–5992.
51 D. K. Britt, H. Furukawa, B. Wang, T. G. Glover and O. M. Yaghi, *Proc. Natl. Acad. Sci. U. S. A.*, 2009, **106**, 20637–20640.
52 T. Devic, P. Horcajada, C. Serre, F. Salles, G. Maurin, B. Moulin, D. Heurtaux, G. Clet, A. Vimont and J. M. Greneche, *J. Am. Chem. Soc.*, 2010, **132**, 1127–1136.
53 S. Yang, A. J. Ramirez-Cuesta, R. Newby, V. Garcia-Sakai, P. Manuel, S. K. Callear, S. I. Campbell, C. C. Tang and M. Schröder, *Nat. Chem.*, 2015, **7**, 121–129.
54 Y.-L. Huang, P.-L. Qiu, H. Zeng, H. Liu, D. Luo, Y. Y. Li, W. Lu and D. Li, *Eur. J. Inorg. Chem.*, 2019, **2019**, 4205–4210.
55 M. H. Mohamed, Y. Yang, L. Li, S. Zhang, J. P. Ruffley, A. G. Jarvi, S. Saxena, G. Veser, J. K. Johnson and N. L. Rosi, *J. Am. Chem. Soc.*, 2019, **141**, 13003–13007.

56 V. F. D. Martins, A. M. Ribeiro, A. F. P. Ferreira, U. Lee, Y. K. Hwang, J. Chang, J. M. Loureiro and A. E. Rodrigues, *Sep. Purif. Technol.*, 2015, **149**, 445–456.

57 S. Xiang, W. Zhou, Z. Zhang, M. A. Green, Y. Liu and B. Chen, *Angew. Chem., Int. Ed.*, 2010, **49**, 4615–4618.

58 J. Pang, F. Jiang, M. Wu, C. Liu, K. Su, W. Lu, D. Yuan and M. Hong, *Nat. Commun.*, 2015, **6**, 7575–7575.

59 Y. He, R. Krishna and B. Chen, *Energy Environ. Sci.*, 2012, **5**, 9107–9120.

60 F. Luo, C. Yan, L. Dang, R. Krishna, W. Zhou, H. Wu, X. Dong, Y. Han, T. Hu and M. Okeeffe, *J. Am. Chem. Soc.*, 2016, **138**, 5678–5684.

61 S. J. Geier, J. A. Mason, E. D. Bloch, W. L. Queen, M. R. Hudson, C. M. Brown and J. R. Long, *Chem. Sci.*, 2013, **4**, 2054–2061.

62 Y.-S. Bae, C. Y. Lee, K. C. Kim, O. K. Farha, P. Nickias, J. T. Hupp, S. T. Nguyen and R. Q. Snurr, *Angew. Chem., Int. Ed.*, 2012, **51**, 1857–1860.

63 E. D. Bloch, W. L. Queen, R. Krishna, J. M. Zadrozny, C. M. Brown and J. R. Long, *Science*, 2012, **335**, 1606–1610.

64 L. Li, R. Lin, R. Krishna, H. Li, S. Xiang, H. Wu, J. Li, W. Zhou and B. Chen, *Science*, 2018, **362**, 443–446.

65 B. Li, Y. Zhang, R. Krishna, K. X. Yao, Y. Han, Z. Wu, D. Ma, Z. Shi, T. Pham and B. Space, *J. Am. Chem. Soc.*, 2014, **136**, 8654–8660.

66 Y. Zhang, B. Li, R. Krishna, Z. Wu, D. Ma, Z. Shi, T. Pham, K. Forrest, B. Space and S. Ma, *Chem. Commun.*, 2015, **51**, 2714–2717.

67 S. Yang, A. J. Ramirezcuesta, R. Newby, V. Garciasakai, P. Manuel, S. K. Callear, S. Campbell, C. C. Tang and M. Schroder, *Nat. Chem.*, 2015, **7**, 121–129.

68 X. Cui, K. Chen, H. Xing, Q. Yang, R. Krishna, Z. Bao, H. Wu, W. Zhou, X. Dong and Y. Han, *Science*, 2016, **353**, 141–144.

69 P. Liao, W. Zhang, J. Zhang and X. Chen, *Nat. Commun.*, 2015, **6**, 8697–8697.

70 W. Liang, F. Xu, X. Zhou, J. Xiao, Q. Xia, Y. Li and Z. Li, *Chem. Eng. Sci.*, 2016, **148**, 275–281.

71 Y. Chen, Z. Qiao, H. Wu, D. Lv, R. Shi, Q. Xia, J. Zhou and Z. Li, *Chem. Eng. Sci.*, 2018, **175**, 110–117.

72 R. Lin, H. Wu, L. Li, X. Tang, Z. Li, J. Gao, H. Cui, W. Zhou and B. Chen, *J. Am. Chem. Soc.*, 2018, **140**, 12940–12946.

73 O. T. Qazvini, R. Babarao, Z. Shi, Y. Zhang and S. G. Telfer, *J. Am. Chem. Soc.*, 2019, **141**, 5014–5020.

74 J. Pei, J. Wang, K. Shao, Y. Yang, Y. Cui, H. Wu, W. Zhou, B. Li and G. Qian, *J. Mater. Chem. A*, 2020, **8**, 3613–3620.

75 S. Yuan, L. Zou, H. Li, Y.-P. Chen, J. Qin, Q. Zhang, W. Lu, M. B. Hall and H.-C. Zhou, *Angew. Chem., Int. Ed.*, 2016, **55**, 10776–10780.

76 M. Yu, B. Space, D. M. Franz, W. Zhou, C. He, L. Li, R. Krishna, Z. Chang, W. Li and T. Hu, *J. Am. Chem. Soc.*, 2019, **141**, 17703–17712.

77 H. Zeng, M. Xie, Y.-L. Huang, Y. Zhao, X.-J. Xie, J.-P. Bai, M.-Y. Wan, R. Krishna, W. Lu and D. Li, *Angew. Chem., Int. Ed.*, 2019, **58**, 8515–8519.

78 Z. Chang, D. Yang, J. Xu, T. Hu and X. Bu, *Adv. Mater.*, 2015, **27**, 5432–5441.

79 Y.-P. Li, Y. Wang, Y.-Y. Xue, H.-P. Li, Q.-G. Zhai, S.-N. Li, Y.-C. Jiang, M.-C. Hu and X. Bu, *Angew. Chem., Int. Ed.*, 2019, **58**, 13590–13595.

80 X. Zhao, X. Bu, Q. Zhai, H. Tran and P. Feng, *J. Am. Chem. Soc.*, 2015, **137**, 1396–1399.

81 X. Zhao, X. Bu, E. T. Nguyen, Q. Zhai, C. Mao and P. Feng, *J. Am. Chem. Soc.*, 2016, **138**, 15102–15105.

82 Q. Zhai, X. Bu, C. Mao, X. Zhao, L. L. Daemen, Y. Cheng, A. J. Ramirezcuesta and P. Feng, *Nat. Commun.*, 2016, **7**, 13645.

83 Q. Zhai, X. Bu, X. Zhao, D. Li and P. Feng, *Acc. Chem. Res.*, 2017, **50**, 407–417.

84 Y. Ye, Z. Ma, R. Lin, R. Krishna, W. Zhou, Q. Lin, Z. Zhang, S. Xiang and B. Chen, *J. Am. Chem. Soc.*, 2019, **141**, 4130–4136.

85 X. Duan, Q. Zhang, J. Cai, Y. Yang, Y. Cui, Y. He, C. Wu, R. Krishna, B. Chen and G. Qian, *J. Mater. Chem. A*, 2014, **2**, 2628–2633.

86 Y. He, Z. Zhang, S. Xiang, H. Wu, F. R. Fronczek, W. Zhou, R. Krishna, M. Okeeffe and B. Chen, *Chem. – Eur. J.*, 2012, **18**, 1901–1904.

87 Y. He, Z. Zhang, S. Xiang, F. R. Fronczek, R. Krishna and B. Chen, *Chem. Commun.*, 2012, **48**, 6493–6495.

88 H.-G. Hao, Y.-F. Zhao, D.-M. Chen, J.-M. Yu, K. Tan, S. Ma, Y. Chabal, Z.-M. Zhang, J.-M. Dou, Z.-H. Xiao, G. Day, H.-C. Zhou and T.-B. Lu, *Angew. Chem., Int. Ed.*, 2018, **57**, 16067–16071.

89 K. Chen, D. G. Madden, S. Mukherjee, T. Pham, K. A. Forrest, A. Kumar, B. Space, J. Kong, Q. Zhang and M. J. Zaworotko, *Science*, 2019, **366**, 241–246.

90 J. B. James, L. Lang, L. Meng and J. Y. S. Lin, *ACS Appl. Mater. Interfaces*, 2020, **12**, 3893–3902.

91 H. Bux, C. Chmelik, R. Krishna and J. Caro, *J. Membr. Sci.*, 2011, **369**, 284–289.

92 S. Qiu, M. Xue and G. Zhu, *Chem. Soc. Rev.*, 2014, **43**, 6116–6140.

93 L. Boudjema, E. Mamontova, J. Long, J. Larionova, Y. Guari and P. Trens, *Inorg. Chem.*, 2017, **56**, 7598–7601.

94 J. Canivet, A. Fateeva, Y. Guo, B. Coasne and D. Farrusseng, *Chem. Soc. Rev.*, 2014, **43**, 5594–5617.